AGU PUBLICATIONS

Geochemistry, Geophysics, Geosystems

RESEARCH ARTICLE
10.1002/2014GC005291

Special Section:
Magnetism From Atomic to Planetary Scales: Physical Principles and Interdisciplinary Applications in Geo- and Planetary Sciences

Key Points:
- First-order reversal curve central ridges carry magnetofossil information
- Central ridge form varies within and between different sediment sequences
- Central ridge magnetofossil characterization provides environmental information

Supporting Information:
- Supplementary data
- Readme

Correspondence to:
D. Heslop,
david.heslop@anu.edu.au

Citation:
Heslop, D., A. P. Roberts, and L. Chang (2014), Characterizing magnetofossils from first-order reversal curve (FORC) central ridge signatures, *Geochem. Geophys. Geosyst.*, *15*, 2170–2179, doi:10.1002/2014GC005291.

Received 10 FEB 2014
Accepted 27 APR 2014
Accepted article online 2 MAY 2014
Published online 4 JUN 2014

Characterizing magnetofossils from first-order reversal curve (FORC) central ridge signatures

David Heslop[1], Andrew P. Roberts[1], and Liao Chang[1]

[1]Research School of Earth Sciences, Australian National University, Canberra, ACT, Australia

Abstract The central ridge structure of a first-order reversal curve (FORC) distribution is indicative of uniaxial noninteracting single domain magnetic particles, which provides the opportunity to identify and characterize biogenic magnetic mineral remains (magnetofossils) in sediments. Recent studies have shown that magnetofossils are widespread in the geological record and that they carry useful environmental information and contribute to paleomagnetic recording, which makes it essential to quantify how these biogenic components contribute to the magnetic properties of sediments. We present results from six sedimentary sequences whose magnetic mineral assemblages contain a significant magnetofossil contribution. Using principal component analysis, we find that the central ridge properties exhibit both intra-sequnce and inter-sequence variability that may be ascribed to external environmental factors. While samples from individual sediment sequences tend to cluster together, there is a continuum of inter-sequence behavior that appears to be related to a variety of magnetofossil properties. We demonstrate the complexity of biogenic magnetic components in sedimentary environments, but also the power and potential of FORC central ridges for understanding magnetic mixtures and unraveling environmental information.

1. Introduction

Magnetotactic bacteria synthesize chains of permanent nanomagnets, which provide a means to orient themselves using Earth's magnetic field and locate optimal living conditions [*Blakemore*, 1975; *Blakemore et al*., 1980; *Kirschvink*, 1980; *Bazylinski and Frankel*, 2004; *Simmons et al*., 2006]. The efficiency of this magnetotaxis process is increased through synthesis of magnetite or greigite crystals that occur in the ideal stable single domain (SSD) magnetic size range with high spontaneous magnetization [*Kopp and Kirschvink*, 2008; *Muxworthy and Williams*, 2009]. In recent years, several techniques have been developed to identify, characterize, and quantify different magnetofossil (the inorganic remains of magnetotactic bacteria) populations within sedimentary magnetic mineral assemblages. It has been shown that both magnetofossil morphology and abundance respond to environmental factors and, thus, have potential to act as paleoclimatic and paleoceanographic proxies [*Hesse*, 1994; *Lean and McCave*, 1998; *Yamazaki and Kawahata*, 1998; *Just et al*., 2012; *Roberts et al*., 2011; *Yamazaki*, 2012].

When suitable preservation conditions exist in sediments, magnetofossils can carry paleomagnetic information [*Tarduno et al*., 1998; *Abrajevitch and Kodama*, 2009; *Roberts et al*., 2012; *Heslop et al*., 2013; *Roberts et al*., 2013a]. Under some circumstances, however, the contribution of magnetofossils to sedimentary remanent magnetizations can be detrimental to the recovery of high-fidelity paleomagnetic information. For example, variations in magnetofossil magnetic properties and relative abundance through time violate the assumption of a constant magnetic mineralogy that is essential to estimate sedimentary relative paleointensities [*Tauxe*, 1993; *Roberts et al*., 2013b; *Yamazaki et al*., 2013]. Additionally, if magnetotactic bacteria lived below the sedimentary surface mixed layer, they can give rise to a biogeochemical remanent magnetization that is much younger than the sediments that host the magnetofossils, which will complicate paleomagnetic recording [*Tarduno et al*., 1998; *Abrajevitch and Kodama*, 2009; *Roberts et al*., 2013a].

Given the important environmental information carried by magnetofossils and their contribution to paleomagnetic recording, it is essential to understand the natural variability of their magnetic properties. Our current interpretational framework for identifying magnetofossils depends on recognition of discrete biogenic components with different coercivities [*Egli*, 2004]. Magnetically distinct groups of magnetofossils were identified by *Egli* [2004] in both lacustrine and marine settings and have now been reported in a variety of sediments [*Kodama et al*., 2013; *Lascu and Plank*, 2013; *Ludwig et al*., 2013; *Roberts et al*., 2013a]. *Egli* [2004]

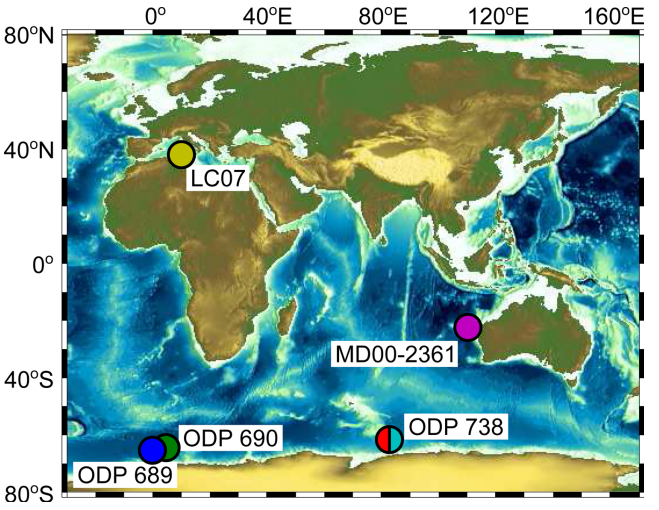

Figure 1. Location map of the studied cores. Relevant details of the locations are given in the main text, section 2.

proposed the existence of biogenic soft (BS) and biogenic hard (BH) components, which he interpreted to correspond to different magnetosome morphologies whose presence is controlled by environmental factors. Additionally, *Egli* [2004] demonstrated that the coercivity distributions of biogenic magnetic components in marine and freshwater sediments could be different, again supporting the idea that magnetofossil properties reflect the respective environmental setting. Subsequent studies have tested this hypothesized dependency using transmission electron microscope (TEM) imaging to draw links between magnetofossil morphology and coercivity [*Yamazaki and Ikehara*, 2012; *Lascu and Plank*, 2013]. An open question remains, however, as to the level of natural variability that can be expected in the properties of different magnetofossil components and their combined populations.

First-order reversal curve (FORC) diagrams provide detailed information concerning the distribution of coercivities and interaction fields in fine magnetic particle systems [*Pike et al*., 1999; *Roberts et al*., 2000]. *Pike et al*. [1999] demonstrated that magnetically noninteracting SSD particles produce a characteristic ridge along the coercivity (B_c) axis of a FORC distribution. An exact FORC model for randomly oriented, noninteracting, elongated SSD particles exhibiting coherent rotation of magnetization with changing applied field was provided by *Newell* [2005], which demonstrates that such an SSD assemblage would produce an infinitely sharp ridge along the B_c axis, corresponding to the switching fields of individual particles. In turn, *Egli et al*. [2010] developed an experimental protocol to measure and isolate this feature, termed the "central ridge", from a high-resolution FORC distribution.

FORC central ridges are indicative of noninteracting SSD particles and, therefore, are well suited to isolate the contribution of magnetofossils to mixed magnetic mineral assemblages. While the model of *Newell* [2005] considered isolated SSD particles, the individual crystals in magnetosome chains are flux linked so that the whole chain behaves like an elongated SSD particle [*Penninga et al*., 1995; *Dunin-Borkowski et al*., 1998; *Hanzlik et al*., 2002; *Muxworthy et al*., 2006; *Muxworthy and Williams*, 2009]. Thus, although the individual magnetic particles in a chain interact strongly with their neighbors, they will still contribute to the narrow central ridge because the measured response is for the entire chain, which does not interact with other chains. These insights have made the FORC central ridge a key tool for remote sensing of magnetofossils [*Yamazaki*, 2009; *Roberts et al*., 2011, 2012, 2013a; *Larrasoaña et al*., 2012; *Yamazaki*, 2012; *Channell et al*., 2013; *Heslop et al*., 2013; *Ludwig et al*., 2013]. In many cases, however, even if a FORC distribution contains a statistically significant central ridge [*Heslop and Roberts*, 2012a], the presence of biogenic magnetic particles is best confirmed by TEM imaging.

Using marine sediment samples that are known to contain magnetofossils, we have investigated the different biogenic contributions to FORC central ridges. We present a principal component analysis (PCA) that elucidates the internal structure of the central ridge data set and allows the relationship between different samples and sediment sequences to be visualized. Our aim is to facilitate extraction of as much information as possible from FORC central ridges and to enable more complete interpretation of sedimentary magnetic particle assemblages.

2. Sample Material

Thirty-seven samples were selected from three locations in the Southern Ocean (Figure 1). Ocean Drilling Program (ODP) Site 738 (62°42.54′S, 82°47.25′E; 2253 m water depth) is located on the southern Kerguelen

Plateau. Pelagic biogenic oozes were sampled through Eocene (20.65–41.55 mbsf) and Paleocene-Eocene Thermal Maximum (PETM; 284.46–285.78 mbsf) intervals in Holes 738B and 738C, respectively. Earlier magnetic analyses of these sediments, including high-resolution FORCs, were reported by *Roberts et al*. [2011, 2012, 2013a], *Heslop and Roberts* [2012b], and *Larrasoaña et al*. [2012]. TEM imaging has confirmed the presence of magnetofossils throughout these studied intervals [*Roberts et al*., 2011; *Larrasoaña et al*., 2012]. Pelagic sediments were also analyzed from Maud Rise (Weddell Sea) at ODP Holes 689D (64°31.01′S, 3°06.00′E, 2080 m water depth) and 690C (65°09.62′S, 1°12.29′E, 2914 m water depth). Samples were selected from Eocene-Oligocene sediments that are dominated by biogenic ooze with a small terrigenous contribution. Magnetic analyses of these samples, some of which included high-resolution FORCs, have been reported by *Florindo and Roberts* [2005], *Heslop and Roberts* [2012b], *Roberts et al*. [2012], and *Chang et al*. [2013]. TEM observations have confirmed the presence of magnetofossils in the selected interval from ODP Hole 689D [*Roberts et al*., 2012].

Piston core LC07 was recovered from the western Sicily Strait in the Mediterranean Sea (38°08.72′N, 10°04.73′E, 488 m water depth) and spans the last 1 million years [*Dinarès-Turell et al*., 2002, 2003]. The sediments consist of foraminifer-rich mud and nannofossil ooze with a homogeneous grey to olive-grey color. Environmental magnetic results and TEM images from these sediments [*Dinarès-Turell et al*., 2003] conclusively demonstrate the presence of magnetofossils. High-resolution FORC diagrams for a subset of LC07 samples contain sharply defined central ridges produced by noninteracting SSD grains [*Roberts et al*., 2012]. Five samples from core LC07 were selected for this study.

Core MD00-2361 consists of Late Quaternary sediments recovered from offshore northwestern Australia (22°04.92′S, 113°28.63′E, 1805 m water depth). The sediments of core MD00-2361 alternate between interglacial intervals rich in fluvially supplied detritus and carbonate-rich glacial periods that are enriched in eolian detritus [*Gingele et al*., 2001; *Gingele and De Deckker*, 2004; *Spooner et al*., 2011; *Stuut et al*., 2014]. A rock magnetic investigation, including high-resolution FORC diagrams and TEM imaging, reported by *Heslop et al*. [2013] demonstrated that magnetofossils are present throughout core MD00-2361, but that they dominate the magnetic mineral assemblage during glacial intervals. For this study, four samples (two glacial, two interglacial) were selected from core MD00-2361.

3. Methods

Hysteresis loops, backfield demagnetization curves and FORC measurements were performed with Princeton Measurements Cooperation vibrating sample magnetometers at various institutions. FORC measurements were made following the high-resolution measurement protocol defined by *Egli et al*. [2010] and FORC distributions were calculated using the VARIFORC method of *Egli* [2013] with smoothing parameters appropriate for samples containing a central ridge ($s_{c,0} = 7$, $s_{b,0} = 3$, $s_{c,1} = s_{b,1} = 7$, and $\lambda = 0.07$). All FORC measurements were processed with the same smoothing parameters to ensure consistency. Thus, although the selected smoothing parameters may not have been optimal for a given sample, they were deemed optimal for the ensemble of all samples. Where necessary, weakly magnetized samples were measured repeatedly and the measurements averaged to increase the signal-to-noise ratio.

Central ridge signatures were extracted from the measured FORC distributions using the approach of *Egli et al*. [2010]. This involved constrained least squares fitting [*Lawson and Hanson*, 1974] of vertical profiles through each FORC distribution to separate the Gaussian-like central ridge feature from a continuous background produced by a combination of interacting SSD particles, larger pseudosingle domain and multidomain particles and reversible SSD contributions. To compensate for inter-sample differences in magnetic mineral concentration, each extracted central ridge was normalized to sum to unity. The normalized central ridges were combined into a single matrix (one central ridge per row), centered (each column has its mean subtracted), and subjected to PCA using the singular value decomposition-based MATLAB *princomp* function.

Ludwig et al. [2013] noted that FORC central ridges may not provide a full representation of the entire magnetofossil population within a magnetic mineral assemblage. For example, magnetosome chains may undergo postmortem collapse [*McNeill and Kirschvink*, 1993], producing interactions that result in vertical spreading of the FORC distribution away from the central ridge [*Kind et al*., 2011; *Li et al*., 2012]. Alternatively, some magnetotactic bacteria contain more than one magnetosome chain [*Hanzlik et al*., 2002]. If

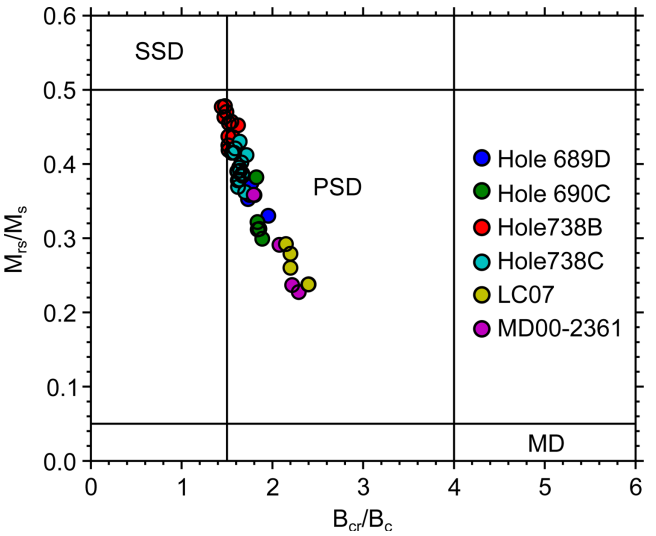

Figure 2. "Day plot" [*Day et al*., 1977] for the 46 studied sediment samples. The data follow a trend through the pseudosingle domain (PSD) field toward the multidomain (MD) field, which is consistent with the sedimentary magnetic mineral assemblages being composed of SSD magnetofossils and coarser detrital particles.

these magnetofossils retain their original configuration after burial they may not contribute to the FORC central ridge.

4. Results

The hysteresis characteristics of the complete sample set are shown in a "Day plot" [*Day et al*., 1977] (Figure 2). The samples form a narrow distribution that trends from close to the SSD field to the center of the pseudosingle domain (PSD) field. Such a trend is indicative of magnetic mineral assemblages that contain mixtures of SSD and coarser particles [*Dunlop*, 2002; *Heslop and Roberts*, 2012b] and is characteristic of sediments that contain varying abundances of magnetofossils [*Roberts et al*., 2012].

The 46 analyzed sediment samples all exhibit clear FORC central ridge signatures, which confirms that their magnetic mineral assemblages contain significant proportions of noninteracting SSD particles (Figure 3). The majority of the FORC distributions contain vertical spreading at low B_c values, which is attributed to both inter-particle magnetic interactions and the presence of large (PSD and multidomain) detrital magnetic particles. While some of the extracted central ridges still contain a clear contribution from measurement noise (e.g., LC07, Figure 3j), inspection of their forms reveals both intra-sequence and inter-sequence variability. PCA [*Jolliffe*, 2002] helps to elucidate the internal structure of the collection of central ridges by representing the data through a combination of linearly uncorrelated *loadings* (the principal component coefficients) and *scores* (the location of individual central ridges in the principal component space). Thus, PCA provides an alternative coordinate system in which the largest mode of data variability is projected onto the first principal component, the second greatest mode of variability is projected onto the second coordinate, etc. Here the first two principal components explain >95% of the total variance of the central ridge data set (Figure 4). Given this high value, we discard the remaining principal components and investigate the internal structure of the central ridge data set based on the representation provided by the leading two principal components. Such a low-rank approximation is advantageous because it is simple to visualize and is not unduly influenced by measurement noise (which will predominantly reside in the discarded principal components).

Principal component scores of the individual central ridges are shown in Figure 5. The samples from the studied sediment sequences cluster in a coherent manner, although with some intra-sequence variability. To help illustrate the properties of the score space, skewed generalized Gaussian (SGG) mixing models for three components [*Egli*, 2003, 2004] were estimated (in log field space) for four points (A-D) located on the two principal components. Following earlier analyses of magnetic mineral assemblages dominated by magnetofossils, the three fitted SGG components are thought to represent the noninteracting SSD fraction of the detrital and extracellular (D+EX) particle assemblages and two separate biogenic components with low and high coercivities [*Egli*, 2004; *Yamazaki*, 2012; *Yamazaki and Ikehara*, 2012; *Ludwig et al*., 2013]. While such mixing models can suffer from nonuniqueness, they are employed here only to demonstrate principal component trends, which are based solely on the central ridge data set.

The principal component loadings map the normalized central ridges to the principal component scores. To demonstrate the relationship between the two leading principal components, we plot them against each other (Figure 6a) to illustrate how they coevolve from low to high fields. The loadings have a smooth trend

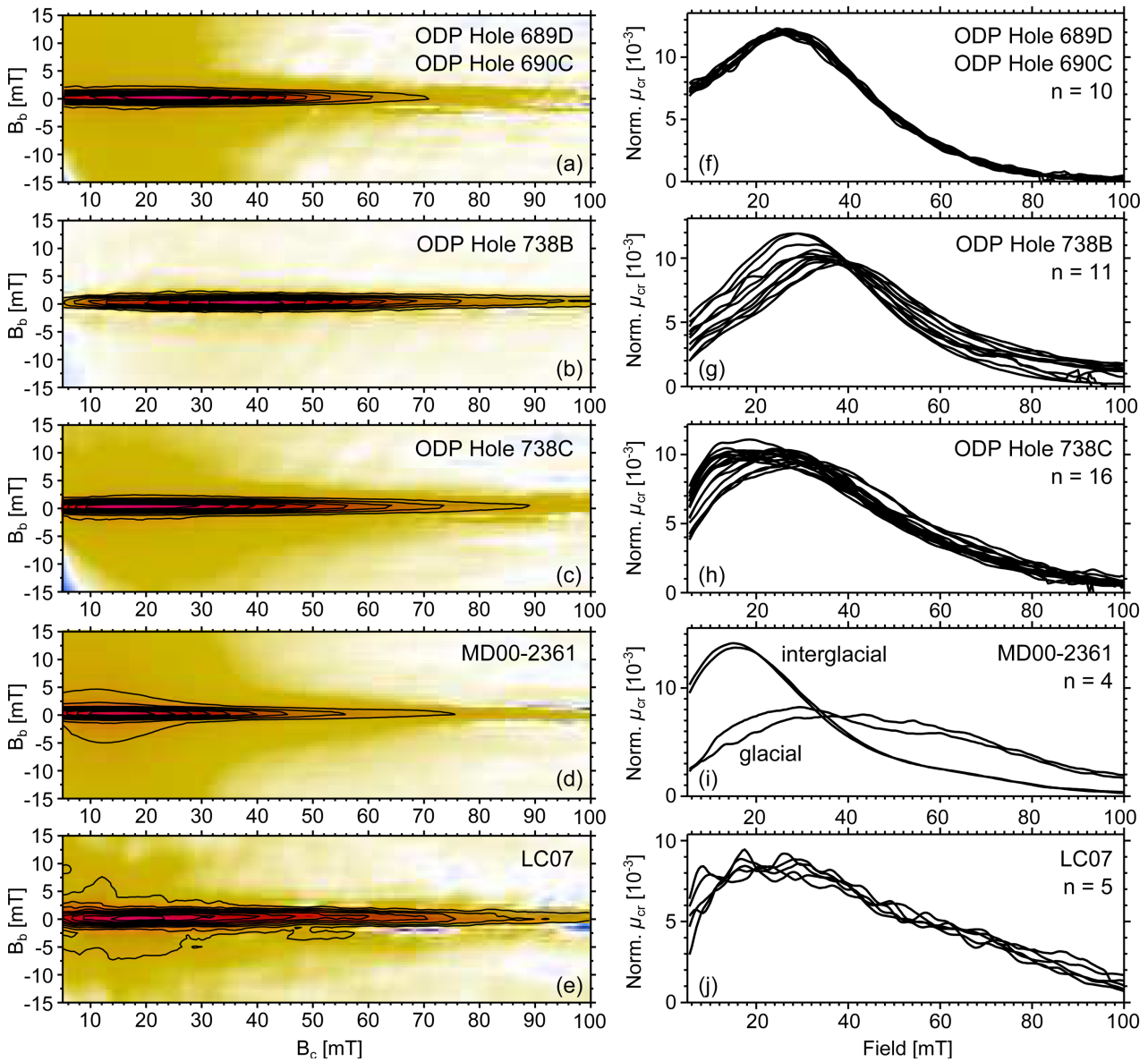

Figure 3. (a–e) Example high-resolution FORC distributions from each of the studied sites calculated using the VARIFORC algorithm [*Egli*, 2013] with parameters suitable for FORC distributions that contain a central ridge ($s_{c,0} = 7$, $s_{b,0} = 3$, $s_{c,1} = s_{b,1} = 7$, and $\lambda = 0.07$). Central ridges (f–j) were extracted from the 46 FORC distributions using the method of *Egli et al.* [2010]. Some of the FORC distributions exhibit smoothing artifacts at high coercivities (e.g., Figure 3a); however, the extraction technique developed by *Egli et al.* [2010] helps to protect against these features being included in the estimated central ridges. The noisy nature of some of the central ridges is due to measurement noise in the original measurements, for example, Figures 3e and 3j. Each ridge has been normalized so that the data values sum to 1.

that passes from the fourth quadrant at low fields, through the first and second quadrants, to the third quadrant at the highest fields. To illustrate how the field-specific loadings are related to different magnetic mineral contributions, a three-component SGG model was fitted to the central ridge obtained from averaging all 46 samples. The relative contribution of each SGG component to the average central ridge was then calculated as a function of field (Figure 6b). As with the earlier SGG models, this mixing representation may suffer from nonuniqueness, but it provides a qualitative guide to relate the principal component loadings to different magnetic mineral components. For example, low field loadings in the fourth quadrant are expected to predominantly represent a D+EX contribution, the first and second quadrants represent increasing relative contributions from soft and hard biogenic components, while the third quadrant is dominated by a hard biogenic contribution.

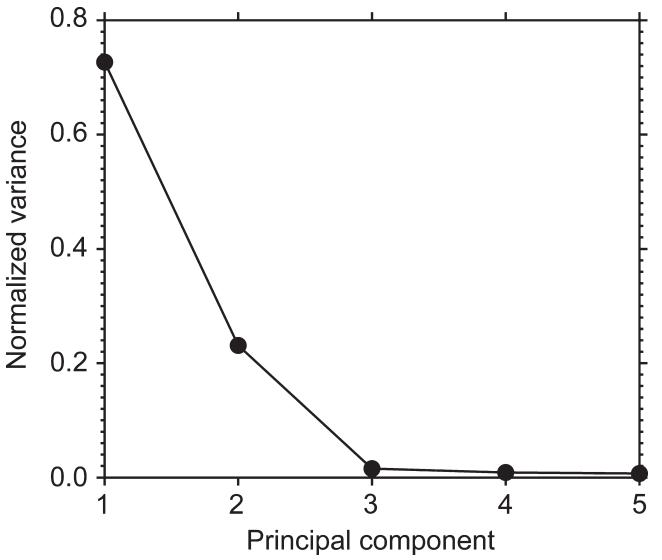

Figure 4. Scree plot of central ridge variance explained by each of the first five principal components. In combination, the leading two principal components (73% and 23%) explain >95% of the total central ridge variance and are, therefore, employed to provide a low-rank representation of the data set.

5. Discussion

Our PCA reveals an apparent continuum of mixtures between a low coercivity D+EX component and biogenic magnetite components and their relative abundances, with varying degrees of intra-sequence variability. Sediments from ODP Holes 689D and 690C have similar central ridges (Figure 3f) and are tightly clustered in the principal component space (Figure 5). Scores for these samples are in the first quadrant, which correspond to a large D+EX component, softer biogenic particles, and a minimal contribution from harder biogenic particles (Figure 5).

Central ridges from ODP Hole 738B have highly variable shapes (Figures 3g and 5), but still occupy an isolated region of the principal component space. Using low-temperature measurements, *Chang et al*. [2013] identified a shift to harder biogenic contributions through the ODP Hole 738B sediment sequence, which they attributed to increased numbers of intact magnetosome chains with elongated morphologies that formed under less oxic conditions. The principal component scores of these less oxic samples are located in the lower part of the second quadrant, while the more oxic sediments are positioned on the boundary between the first and second quadrants (Figure 5). Examination of the loadings (Figure 6a) indicates that the trend observed by *Chang et al*. [2013] is consistent with the principal component representation, which also indicates a shift to biogenic particles with higher coercivities in the less oxic sediments (i.e., a shift from weakly positive to strongly negative scores on the leading principal component).

The PETM samples from ODP Hole 738C lie in a distinct cluster with respect to the younger Eocene samples from ODP Hole 738B (Figure 5). The data trend from the second to the fourth quadrants and correspond to a trend from hard biogenic particles to a relative increase in D+EX particles, respectively. *Larrasoaña et al*. [2012] demonstrated that magnetofossil production and magnetosome grain size varied rapidly through the PETM. Such high-frequency variability would explain the scattered scores for the PETM samples, which follow a different trend to the more oxic-less oxic pattern observed in the younger sediments from ODP Hole 738B.

Samples from Mediterranean core LC07 have scores that plot in the third quadrant and are distinct from the other studied sediment sequences. The LC07 sediments contain a significant detrital magnetite contribution [*Dinarès-Turell et al*., 2003]; however, this component is coarse grained [*Roberts et al*., 2012] and, therefore, will make a minimal contribution to the extracted central ridges. TEM imaging of magnetofossils from LC07 revealed both elongated (e.g., prismatic) and more equant (i.e., cuboidal) morphologies [*Dinarès-Turell et al*., 2003], which are expected to span a range of coercivities [*Phatak et al*., 2011; *Lascu and Plank*, 2013]. The location of the LC07 data in principal component space implies a magnetic assemblage with a relatively abundant hard biogenic component, which is consistent with the LC07 central ridges extending to high fields (Figure 3j). The relatively tight clustering of the LC07 scores indicates that the samples have similar magnetic mineral contributions to their FORC central ridges. Given the small number of analyzed samples (n = 5), however, it is not currently feasible to attribute any environmental significance to this tight clustering.

Heslop et al. [2013] demonstrated that, while the magnetic mineral assemblage of interglacial sediments from core MD00–2361 contains magnetite magnetofossils, they are dominated by detrital material. In

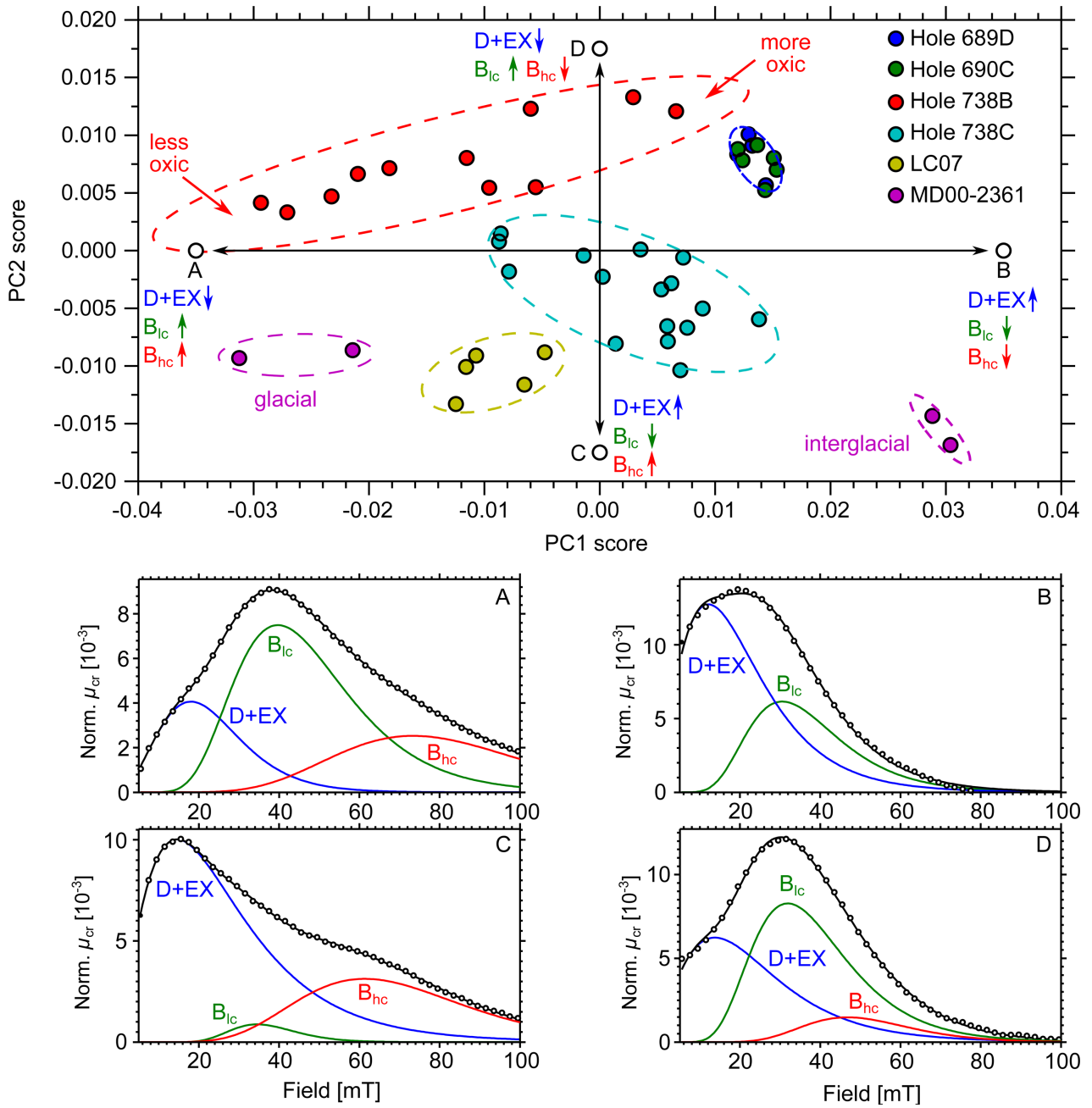

Figure 5. (top) Central ridge scores for the leading two principal components (PC1 and PC2). Ellipses are drawn around collections of points as a general guide and do not have any statistical meaning. Points A, B, C, and D (located along the axes) were selected to demonstrate how central ridge characteristics change through the principal component space. (bottom) Central ridges that correspond to the four positions (A, B, C, and D) are fitted with three-component skewed generalized Gaussian (SGG) models [*Egli*, 2003]. The three SGG curves are used to represent the noninteracting SSD fraction of the D+EX (blue), the lower coercivity biogenic (B_{lc}, green), and the higher coercivity biogenic (B_{hc}, red) components, respectively. Evolution of the magnetic mineral assemblage along PC1 (positions A to B) and PC2 (positions C to D) is shown in the top plot in terms of increasing (upward arrows) and decreasing (downward arrows) relative abundances of the specified components.

contrast, glacial sediments were deposited at times when riverine detrital flux was minimal, and contain a high abundance of magnetofossils. This pattern is consistent with the four analyzed MD00–2361 central ridges, which provide evidence for a large difference between glacial (third quadrant, detrital poor and overall harder biogenic) and interglacial (fourth quadrant, detrital rich and overall softer biogenic) cases. The glacial-interglacial shift in central ridge properties for core MD00–2361 provides a clear example of environmental control on magnetofossil properties.

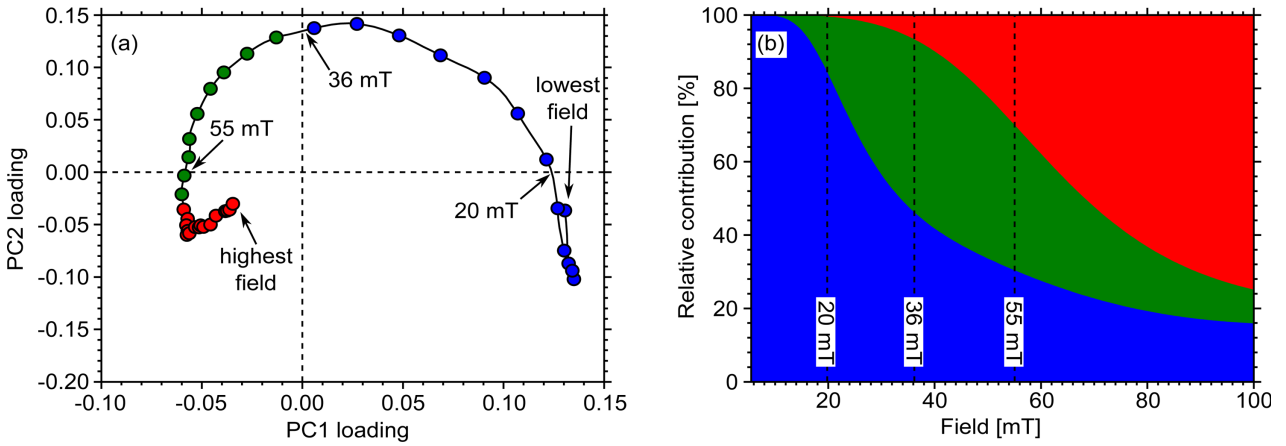

Figure 6. (a) Loadings for the leading two principal components (PC1 and PC2). For clarity, only every fifth data point is shown with a symbol, but the line connecting the symbols contains all data. To show how the loadings evolve between the lowest and highest considered magnetic fields (5.5 and 100 mT, respectively), the magnetic fields at which the loadings pass between quadrants are marked. (b) Relative contributions of three SGG components (blue = D+EX, green = lower coercivity biogenic, and red = higher coercivity biogenic) to the mean central ridge for all studied samples as a function of field. This model provides a basic relationship between magnetic field and the relative abundance of each magnetic mineral component to aid interpretation of the principal component loadings (the points in Figure 6a are color-coded according to which component is dominant in the mean central ridge model). The principal component representation does not assume that the coercivity distributions of the components are fixed; therefore, it is possible for individual components to become harder or softer at different locations in the principal component space.

To summarize, central ridge data from the various studied sediment sequences plot in distinct regions of the principal component space, which indicates that the magnetic properties of biogenic magnetite assemblages are highly variable rather than being fixed. This is supported by the work of *Egli* [2004], who found consistent biogenic soft (BS) and biogenic hard (BH) components across a wide variety of sediments, but also reported lower coercivity biogenic components in marine sediments (attributed to differences in magnetosome morphologies of marine and freshwater magnetotactic bacteria). Additionally, by unmixing isothermal and anhysteretic remanent demagnetization curves, *Lascu and Plank* [2013] demonstrated that magnetofossil components in lake sediments occupy a spectrum of hardnesses with median coercivities spanning ~20–80 mT. On the basis of detailed TEM analysis, *Lascu and Plank* [2013] suggested that the coercivity of different biogenic components is, at least partially, controlled by grain morphology, with equant (elongated) particles being softer (harder). This empirical observation is supported by theoretical calculations, which indicate that shape and separation of individual crystals in magnetosome chains exert a strong control on chain coercivity [*Phatak et al*., 2011]. Allied to magnetosome morphology is chain length, which is difficult to assess in natural sediments because chains are usually disrupted during TEM sample preparation. Micromagnetic calculations for simple chain structures have, however, revealed that magnetosome coercivity will increase rapidly with chain length, but will reach a maximum at lengths of <10 particles [*Muxworthy and Williams*, 2009].

It is apparent that several factors, including magnetofossil morphology, chain length, chain preservation, and postmortem oxidation, could explain the coexistence of multiple, magnetically distinct, biogenic components. TEM imaging of the sediments analyzed in this study revealed biogenic magnetite particles with a variety of typical magnetosome morphologies, including octahedra, elongated prisms, bullets and teardrops, some of which remained arranged in short chains after extraction from the sediment [*Dinarès-Turell et al*., 2003; *Roberts et al*., 2011; *Larrasoaña et al*., 2012; *Roberts et al*., 2012; *Heslop et al*., 2013]. The PCA presented here indicates that such factors, in concert with changes in the relative abundances of different magnetofossil components, can explain both intra-sequence and inter-sequence variability in central ridge form.

If magnetofossil properties, such as magnetosome morphology, are controlled by external environmental factors, further quantification of FORC central ridges has potential for paleoclimatic and paleoceanographic reconstruction [*Hesse*, 1994; *Roberts et al*., 2012; *Chang et al*., 2013]. Additionally, unrecognized changes in magnetofossil type and abundance could have a detrimental effect on interpretation of sedimentary relative paleointensity signals [*Roberts et al*., 2012; *Yamazaki et al*., 2013]. In the context of collections of FORC

distributions for sediment samples, central ridge analysis of the type presented here will be useful for quantifying the influence of such factors on paleomagnetic recording.

6. Conclusions

We have measured and analyzed FORC central ridge signatures for 46 samples from six sediment sequences. In excess of 95% of the central ridge variance is represented by the leading two principal components, which provides a low-rank approximation of both intra-sequence and inter-sequence variability for the studied samples. Data from each sediment sequence occupy a distinct region of the principal component space, which indicates that magnetofossil morphology and abundance are highly variable and are related to local conditions. If magnetofossil properties, such as morphology, are controlled by external environmental factors, further quantification of FORC central ridge signatures could become an important tool for paleoclimatic and paleoceanographic reconstruction [*Hesse*, 1994; *Lean and McCave*, 1998; *Yamazaki and Kawahata*, 1998; *Roberts et al*., 2011; *Chang et al*., 2013]. Additionally, changes in magnetofossil type and abundance could be important for interpretation of sedimentary relative paleointensity signals [*Roberts et al*., 2012; *Yamazaki et al*., 2013]. In the context of collections of sedimentary FORC distributions, central ridge analysis of the type presented here will be useful for quantifying the influence of these factors on paleomagnetic recording.

Acknowledgments
This work was supported by the Australian Research Council (grant DP120103952). We are grateful to Toshi Yamazaki and an anonymous reviewer for constructive comments that helped to improve the final manuscript. The central ridge data and principal component analysis solution produced in this work are available as a supporting information file.

References

Abrajevitch, A., and K. Kodama (2009), Biochemical vs. detrital mechanism of remanence acquisition in marine carbonates: A lesson from the K-T boundary interval, *Earth Planet. Sci. Lett.*, *286*, 269–277.
Bazylinski, D. A., and R. B. Frankel (2004), Magnetosome formation in prokaryotes, *Nat. Rev. Microbiol.*, *2*, 217–230.
Blakemore, R. P. (1975), Magnetotactic bacteria, *Science*, *190*, 377–379.
Blakemore, R. P., R. B. Frankel, and A. J. Kalmijn (1980), South-seeking magnetotactic bacteria in the Southern Hemisphere, *Science*, *286*, 384–385.
Chang, L., M. Winklhofer, A. P. Roberts, D. Heslop, F. Florindo, M. J. Dekkers, W. Krijgsman, K. Kodama, and Y. Yamamoto (2013), Low-temperature magnetic properties of pelagic carbonates: Oxidation of biogenic magnetite and identification of magnetosome chains, *J. Geophys. Res.*, *118*, 1–17, doi:10.1002/2013JB010381.
Channell, J. E. T., C. Ohneiser, Y. Yamamoto, and M. S. Kesler (2013), Oligocene-Miocene magnetic stratigraphy carried by biogenic magnetite at sites U1334 and U1335 (equatorial Pacific Ocean), *Geochem. Geophys. Geosyst.*, *14*, 265–282, doi:10.1029/2012GC004429.
Day, R., M. Fuller, and V. A. Schmidt (1977), Hysteresis properties of titanomagnetites: Grain-size and compositional dependence, *Phys. Earth Planet. Inter.*, *13*, 260–267, doi:10.1016/0031-9201(77)90108-X.
Dinarès-Turell, J., L. Sagnotti, and A. P. Roberts (2002), Relative geomagnetic paleointensity from the Jaramillo subchron to the Matuyama/Brunhes boundary as recorded in a Mediterranean piston core, *Earth Planet. Sci. Lett.*, *194*, 327–341.
Dinarès-Turell, J., B. A. A. Hoogakker, A. P. Roberts, E. J. Rohling, and L. Sagnotti (2003), Quaternary climatic control of biogenic magnetite production and eolian dust input in cores from the Mediterranean Sea, *Palaeogeogr. Palaeoclimatol. Palaeoecol.*, *190*, 195–209.
Dunin-Borkowski, R. E., M. R. McCartney, R. B. Frankel, D. A. Bazylinski, M. Pósfai, and P. R. Buseck (1998), Magnetic microstructure of magnetotactic bacteria by electron holography, *Science*, *282*, 1868–1870.
Dunlop, D. J. (2002), Theory and application of the Day plot (M_{rs}/M_s versus H_{cr}/H_c): 1. Theoretical curves and tests using titanomagnetite data, *J. Geophys. Res.*, *107*(B3), 2056, doi:10.1029/2001JB000486.
Egli, R. (2003), Analysis of the field dependence of remanent magnetization curves, *J. Geophys. Res.*, *108*(B2), 2081, doi:10.1029/2002JB002023.
Egli, R. (2004), Characterization of individual rock magnetic components by analysis of remanence curves, 1. Unmixing natural sediments, *Stud. Geophys. Geod.*, *48*, 391–446.
Egli, R. (2013), VARIFORC: An optimized protocol for calculating non-regular first-order reversal curve (FORC) diagrams, *Global Planet. Change*, *110*, 302–320.
Egli, R., A. P. Chen, M. Winklhofer, K. P. Kodama and C.-S. Horng (2010), Detection of noninteracting single domain particles using first-order reversal curve diagrams, *Geochem. Geophys. Geosyst.*, *11*, Q01Z11, doi:10.1029/2009GC002916.
Florindo, F., and A. P. Roberts (2005), Eocene-Oligocene magnetobiostratigraphy of ODP sites 689 and 690, Maud Rise, Weddell Sea, Antarctica, *Geol. Soc. Am. Bull.*, *117*, 46–66, doi:10.1130/B25541.1.
Gingele, F. X., and P. De Deckker (2004), Fingerprinting Australia's rivers with clay minerals and the application for the marine record of climate change, *Aust. J. Earth Sci.*, *51*, 339–348.
Gingele, F. X., P. De Deckker, and C. D. Hillenbrand (2001), Clay mineral distribution in surface sediments between Indonesia and NW Australia—Source and transport by ocean currents, *Mar. Geol.*, *179*, 135–146.
Hanzlik, M., M. Winklhofer, and N. Petersen (2002), Pulsed-field-remanence measurements on individual magnetotactic bacteria, *J. Magn. Magn. Mater.*, *248*, 258–267.
Heslop, D., and A. P. Roberts (2012a), Estimation of significance levels and confidence intervals for first-order reversal curve diagrams, *Geochem. Geophys. Geosyst.*, *13*, Q12Z40, doi:10.1029/2009GC002413.
Heslop, D., and A. P. Roberts (2012b), Estimating best-fit binary mixing lines in the Day plot, *J. Geophys. Res.*, *117*, B01101, doi:10.1029/2011JB008787.
Heslop, D., A. P. Roberts, L. Chang, M. Davies, A. Abrajevitch, and P. De Deckker (2013), Quantifying magnetite magnetofossil contributions to sedimentary magnetizations, *Earth Planet. Sci. Lett.*, *382*, 58–65.
Hesse, P. P. (1994), Evidence for bacterial palaeoecological origin of mineral magnetic cycles in oxic and sub-oxic Tasman Sea sediments, *Mar. Geol.*, *117*, 1–17.

Jolliffe, I. T. (2002), *Principal Component Analysis*, 2nd ed., Springer-Verlag, New York, N. Y.
Just, J., M. J. Dekkers, T. von Dobeneck, A. van Hoesel, and T. Bickert (2012), Signatures and significance of aeolian, fluvial, bacterial and diagenetic magnetic mineral fractions in Late Quaternary marine sediments off Gambia, NW Africa, *Geochem. Geophys. Geosyst.*, *13*, Q0AO02, doi:10.1029/2012GC004146.
Kind, J., A. U. Gehring, M. Winklhofer, and A. M. Hirt (2011), Combined use of magnetometry and spectroscopy for identifying magnetofossils in sediments, *Geochem. Geophys. Geosyst.*, *12*, Q08008, doi:10.1029/2011GC003633.
Kirschvink, J. L. (1980), South-seeking magnetic bacteria, *J. Exp. Biol.*, *86*, 345–347.
Kodama, K. P., R. E. Moeller, D. A. Bazylinski, R. E. Kopp, and A. P. Chen (2013), The mineral magnetic record of magnetofossils in recent lake sediments of Lake Ely, PA, *Global Planet. Change*, *110*, 350–363.
Kopp, R. E., and J. L. Kirschvink (2008), The identification and biogeochemical interpretation of fossil magnetotactic bacteria, *Earth Sci. Rev.*, *86*, 42–61.
Larrasoaña, J. C., A. P. Roberts, L. Chang, S. A. Schellenberg, J. D. Fitz Gerald, R. D. Norris, and J. C. Zachos (2012), Magnetotactic bacterial response to Antarctic dust supply during the Palaeocene-Eocene thermal maximum, *Earth Planet. Sci. Lett.*, *333–334*, 122–133, doi:10.1016/j.epsl.2012.04.003.
Lascu, I., and C. Plank (2013), A new dimension to sediment magnetism: Charting the spatial variability of magnetic properties across lake basins, *Global Planet. Change*, *110*, 340–349.
Lawson, C. L., and R. J. Hanson (1974), *Solving Least Squares Problems*, Prentice Hall, Englewood Cliffs, NJ.
Lean, C. M. B., and I. N. McCave (1998), Glacial to interglacial mineral magnetic and palaeoceanographic changes at Chatham Rise, SW Pacific Ocean, *Earth Planet. Sci. Lett.*, *163*, 247–260.
Li, J., W. Wu, Q. Liu, and Y. Pan (2012), Magnetic anisotropy, magnetostatic interactions and identification of magnetofossils, *Geochem. Geophys. Geosyst.*, *13*, Q10Z51, doi:10.1029/2012GC004384.
Ludwig, P., R. Egli, S. Bishop, V. Chernenko, T. Frederichs, G. Rugel, and S. Merchel (2013), Characterization of primary and secondary magnetite in marine sediment by combining chemical and magnetic unmixing techniques, *Global Planet. Change*, *110*, 321–339.
McNeill, D., and J. L. Kirschvink (1993), Early dolomitization of platform carbonates and the preservation of magnetic polarity, *J. Geophys. Res.*, *98*, 7977–7986.
Muxworthy, A. R., and W. Williams (2009), Critical superparamagnetic/single domain grain sizes in interacting magnetite particles: Implications for magnetosome crystals, *J. R. Soc. Interface*, *6*, 1207–1212.
Muxworthy, A. R., J. G. King, and N. Odling (2006), Magnetic hysteresis properties of interacting and non-interacting micron-sized magnetite produced by electron-beam lithography, *Geochem. Geophys. Geosyst.*, *7*, Q07009, doi:10.1029/2006GC001309.
Newell, A. J. (2005), A high-precision model of first-order reversal curve (FORC) functions for single-domain ferromagnets with uniaxial anisotropy, *Geochem. Geophys. Geosyst.*, *6*, Q05,010, doi:10.1029/2004GC000877.
Penninga, I., H. deWaard, B. M. Moskowitz, D. A. Bazylinksi, and R. B. Frankel (1995), Remanence measurements on individual magnetotactic bacteria using a pulsed magnetic field, *J. Magn. Magn. Mater.*, *149*, 279–286.
Phatak, C., R. Pokharel, M. Beleggia, and M. De Graef (2011), On the magnetostatics of chains of magnetic nanoparticles, *J. Magn. Magn. Mater.*, *323*, 2912–2922.
Pike, C. R., A. P. Roberts, and K. L. Verosub (1999), Characterizing interactions in fine magnetic particle systems using first order reversal curves, *J. Appl. Phys.*, *85*, 6660–6667, doi:10.1063/1.370176.
Roberts, A. P., C. R. Pike, and K. L. Verosub (2000), First-order reversal curve diagrams: A new tool for characterizing the magnetic properties of natural samples, *J. Geophys. Res.*, *105*, 28,461–28,475, doi:10.1029/2000JB900326.
Roberts, A. P., F. Florindo, G. Villa, L. Chang, L. Jovane, S. M. Bohaty, J. C. Larrasoaña, D. Heslop, and J. D. Fitz Gerald (2011), Magnetotactic bacterial abundance in pelagic marine environments is limited by organic carbon flux and availability of dissolved iron, *Earth Planet. Sci. Lett.*, *310*, 441–452.
Roberts, A. P., L. Chang, D. Heslop, F. Florindo, and J. C. Larrasoaña (2012), Searching for single domain magnetite in the "pseudo-single-domain" sedimentary haystack: Implications of biogenic magnetite preservation for sediment magnetism and relative paleointensity determinations, *J. Geophys. Res.*, *117*, B08104, doi:10.1029/2012JB009412.
Roberts, A. P., F. Florindo, L. Chang, D. Heslop, L. Jovane, and J. C. Larrasoaña (2013a), Magnetic properties of pelagic marine carbonates, *Earth Sci. Rev.*, *127*, 111–139.
Roberts, A. P., L. Tauxe and D. Heslop (2013b), Magnetic paleointensity stratigraphy and high-resolution Quaternary geochronology: Successes and future challenges, *Quat. Sci. Rev.*, *61*, 1–16.
Simmons, S. L., D. A. Bazylinski, and K. J. Edwards (2006), South-seeking magnetotactic bacteria in the Northern Hemisphere, *Science*, *311*, 371–374.
Spooner, M. I., P. De Deckker, T. T. Barrows, and L. K. Fifield (2011), The behaviour of the Leeuwin Current offshore NW Australia during the last five glacial–interglacial cycles, *Global Planet. Change*, *75*, 119–132.
Stuut, J.-B. W., F. Temmesfeld, and P. De Deckker (2014), A 550 ka record of aeolian activity near North West Cape, Australia: Inferences from grain size distributions and bulk chemistry of SE Indian Ocean deep-sea sediments, *Quat. Sci. Rev.*, *83*, 83–94.
Tarduno, J. A., W. Tian, and S. Wilkison (1998), Biogeochemical remanent magnetization in pelagic sediments of the western equatorial Pacific Ocean, *Geophys. Res. Lett.*, *25*, 3987–3990.
Tauxe, L. (1993), Sedimentary records of relative paleointensity of the geomagnetic field: Theory and practice, *Rev. Geophys.*, *31*, 319–354.
Yamazaki, T. (2009), Environmental magnetism of Pleistocene sediments in the North Pacific and Ontong-Java Plateau: Temporal variations of detrital and biogenic components, *Geochem. Geophys. Geosyst.*, *10*, Q07Z04, doi:10.1029/2009GC002413.
Yamazaki, T. (2012), Paleoposition of the Intertropical Convergence Zone in the eastern Pacific inferred from glacial-interglacial changes in terrigenous and biogenic magnetic mineral fractions, *Geology*, *40*, 151–154.
Yamazaki, T., and M. Ikehara (2012), Origin of magnetic mineral concentration in the Southern Ocean, *Paleoceanography*, *27*, PA2206, doi:10.1029/2011PA002271.
Yamazaki, T., and H. Kawahata (1998), Organic carbon flux controls the morphology of magnetofossils in sediments, *Geology*, *26*, 1064–1066.
Yamazaki, T., Y. Yamamoto, G. Acton, E. P. Guidry, and C. Richter (2013), Rock-magnetic artifacts on long-term relative paleointensity variations in sediments, *Geochem. Geophys. Geosyst.*, *14*, 29–43, doi:10.1029/2012GC004546.